Infrared Spectroscopy of Hydrated Bisulfate Anion Clusters: HSO4−(H2O)(1−16)

ARTICLE *in* JOURNAL OF PHYSICAL CHEMISTRY LETTERS · SEPTEMBER 2011

Impact Factor: 7.46 · DOI: 10.1021/jz200917f

THE JOURNAL OF PHYSICAL CHEMISTRY Letters

LETTER

pubs.acs.org/JPCL

Infrared Spectroscopy of Hydrated Bisulfate Anion Clusters: $HSO_4^-(H_2O)_{1-16}$

Tara I. Yacovitch,[†] Torsten Wende,[‡] Ling Jiang,[‡] Nadja Heine,[‡] Gerard Meijer,[‡] Daniel M. Neumark,[*,†,§] and Knut R. Asmis[*,‡]

[†]Department of Chemistry, University of California, Berkeley, California 94720, United States

[‡]Fritz-Haber-Institut der Max-Planck-Gesellschaft, Faradayweg 4-6, 14195 Berlin, Germany

[§]Chemical Science Division, Lawrence Berkeley National Laboratory, Berkeley, California 94720, United States

Supporting Information

ABSTRACT: Gas-phase infrared photodissociation spectra of the microhydrated bisulfate anions $HSO_4^-(H_2O)_n$, with $n = 1-16$, are reported in the spectral range of 550−1800 cm^{-1}. The spectra show extensive vibrational structure assigned to stretching and bending modes of the bisulfate core, as well as to water bending and librational modes. Comparison with electronic structure calculations suggests that the acidic proton of HSO_4^- is involved in the formation of a hydrogen bond from $n \geq 1$ and that water−water hydrogen bonds form for $n \geq 2$. The water network for the larger clusters forms hydrogen-bonded "bands" about the bisulfate core. The blue shifting of the SOH bending mode from 1193 ($n = 1$) to 1381 cm^{-1} ($n = 12$) accompanied by a dramatic decrease in its IR intensity suggests increased incorporation of the bisulfate hydrogen atom into the hydrogen-bonding network, the first step toward acid dissociation.

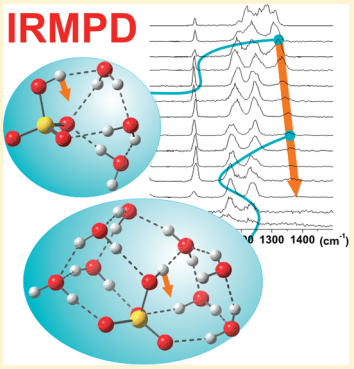

SECTION: Dynamics, Clusters, Excited States

A molecular-level understanding of the solvation of acids in size-selected clusters can lend insight into their behavior in bulk solution. Experimental[1−4] and theoretical[5,6] studies have explored the extent of acid dissociation in clusters and the minimum number of water molecules needed for this process to occur. Analogous experiments on clusters of water with ionic acids (or bases) are also of considerable interest[7,8] because the size and composition of a charged cluster is more readily determined than that for a neutral cluster. This paper focuses on hydrated clusters of the bisulfate anion, HSO_4^-, a weak acid in aqueous solution with a pK_a of 2.0. Bisulfate is also among the most prevalent negative ions in the troposphere and the stratosphere due to its high stability with respect to electron detachment.[9−11] It may also play a role in seeding aerosols by homogeneous nucleation.[9,12−14] These considerations motivate the work presented here, in which we report infrared multiple photon dissociation (IRMPD) spectra of the $HSO_4^-(H_2O)_n$ clusters, $n = 1-16$. This study reports the first vibrational spectra of microhydrated bisulfate and probes the 550−1800 cm^{-1} spectral region, directly accessing intra- as well as intermolecular vibrational modes, including the bending and S−O stretching vibrations of the HSO_4^- core. Experiments of this type provide a means of identifying the bisulfate anion in the presence of water molecules and may thus prove useful in characterizing binary H_2SO_4/water aerosols.[15,16]

Experimental spectroscopic information on the bisulfate ion comes predominantly from bulk studies on aqueous sulfuric acid[15,17−21] where, based on the concentration, a majority of dissolved species is present as HSO_4^- and from thin films of sulfuric acid hydrates.[22,23] The interpretation of these spectra is complicated by the presence of counterions and other species in equilibrium. Nonetheless, a number of characteristic bisulfate vibrational frequencies have been identified. Molecular dynamics[24] calculations predict a stronger interaction of the solvating water at the bisulfate hydrogen site than elsewhere on the ion. Electronic structure calculations have yielded geometries for small ion clusters, $HSO_4^-(H_2O)_n$, $n \leq 10$, showing similar solvation motifs with variations in some of the lowest-energy isomers.[24−27] No previous size-selected gas-phase spectroscopic studies exist for these bisulfate clusters, although the bare ion has been characterized by photoelectron spectroscopy[10] and the associated hydrated SO_4^{2-} dianion has been studied experimentally in small[28−31] and large[32,33] clusters.

IRMPD spectra of $HSO_4^-(H_2O)_n$ clusters with $n = 1-12$, 14, and 16 are shown in Figure 1. The spectra are comprised of the bands labeled A−H, which can be assigned by comparison to the bulk spectra,[15,17,18] FTIR of thin films,[22] and previous IRMPD results.[28,29] Peak A is the water bending mode. It is present in all cluster sizes with a frequency ranging from 1659 to 1677 cm^{-1}. This assignment is consistent with previous results on liquid water (1645 cm^{-1}),[18] liquid sulfuric acid/water aerosols (1725 cm^{-1}),[15] and microhydrated sulfate dianion clusters (1674−1735 cm^{-1}).[28,29]

Received: July 7, 2011
Accepted: August 8, 2011

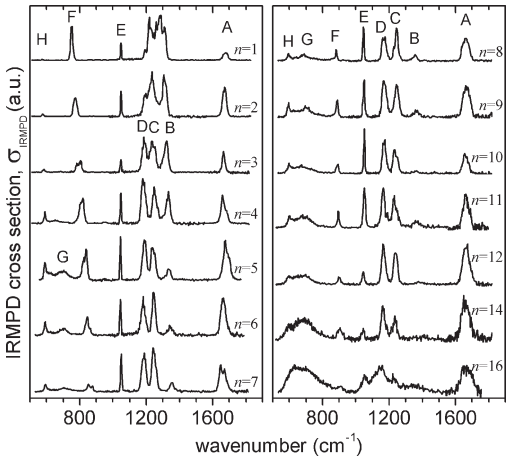

Figure 1. Experimental IRMPD spectra of $HSO_4^-(H_2O)_n$ with n = 1−12, 14, and 16, showing peaks A−H, described and assigned in the text.

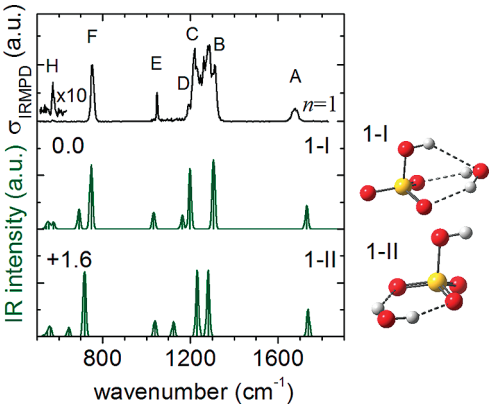

Figure 2. Comparison between the experimental IRMPD spectrum (top black trace) and Gaussian convolution (fwhm = 15 cm^{-1}) of the harmonic MP2/6-311+G** stick spectra of isomers 1-I and 1-II (lower green traces) for n = 1. Structures and their relative energies (in kJ/mol) are also reported.

Peak A increases in intensity and broadens significantly with increasing hydration number. Additional structure such as splitting or shoulders is observed for certain cluster sizes such as n = 4, 5, and 7.

Next is a multiplet of peaks at around 1200 cm^{-1} that evolves into the three peaks B, C, and D by n = 3, as well as peak E at around 1050 cm^{-1}. The vibrations in this region correlate to the triply degenerate antisymmetric stretching mode[28] in tetrahedrally symmetric sulfate, SO_4^{2-}. The T_d symmetry of this anionic center is broken by the presence of the hydrogen in HSO_4^-. The resulting vibrations for a C_{3v} center (the assumed averaged symmetry of bulk aqueous HSO_4^-) are then the symmetric and antisymmetric SO_3 stretches (singly and doubly degenerate, respectively).[22] In C_1 or C_s symmetry, the antisymmetric SO_3 stretch further splits into an antisymmetric SO_2 stretch and a stretching mode of the remaining S═O bond (with some symmetric SO_2 stretching). The S−O−H bend also appears in this region and is coupled to the S═O stretching vibration. The character of the two resulting normal modes and the assignment of the corresponding experimental peaks depend on the degree of hydration, but for $n \geq 3$, peak B corresponds to the SOH bend, C to the S═O stretch, D to the antisymmetric SO_2 stretch, and E to the symmetric SO_3 stretch. These assignments are based on bulk results and calculations discussed below.

With increasing size, peak B increases notably in frequency, from 1321 cm^{-1} for n = 3 to 1381 cm^{-1} for n = 12, and decreases in intensity until it disappears entirely around n = 14. A weak band at 1349 cm^{-1} was previously observed in IR titration experiments of aqueous sulfuric acid solutions[21] (see Figure S11 in Supporting Information) and attributed to a combination band of HSO_4^-. Assuming that this band correlates with band B in our spectra, its assignment to the fundamental of the SOH bend is more likely. In contrast to the bending vibration B, the positions and intensities of peaks C and D stay relatively constant at all levels of hydration, changing only slightly in frequency between n = 3 and 12 from 1235 to 1237 cm^{-1} (peak C) and from 1185 to 1166 cm^{-1} (peak D). Examination of the n = 14 and 16 spectra indicates that the antisymmetric stretch peak D dominates this spectral region. Indeed, condensed-phase measurements show only one broadened peak at 1160 (aerosol), 1190 (solution), 1188 (IR titration), or 1133 cm^{-1} (thin film), which has been assigned to the SO_3 antisymmetric stretching mode of HSO_4^-.[15,17,21,22]

Peak E remains narrow and appears at the same position for all cluster sizes, at an average frequency of 1049 cm^{-1} for n = 1−12. Its assignment to the aforementioned symmetric SO_3 stretch is based on comparison with bulk studies that find frequencies of 1035, 1047, 1051, and 1052 cm^{-1}.[15,17,21,22] The narrow line width and constant frequency indicate that this mode is not affected by the solvent network.

Finally, we turn to peaks F, G, and H in the low-energy region of the spectrum. Peak F is present in all cluster sizes and is the peak that is the most blue-shifted by increasing water coordination (752−910 cm^{-1} from n = 1 to 16). This peak correlates directly to the bisulfate S−OH stretch observed in the condensed-phase measurements at 897 (aerosol), 897 (solution), 887 (IR titration), or 899 cm^{-1} (thin film).[15,17,21,22] After n = 8, additional solvent molecules no longer have an effect on the peak frequency, but some broadening is observed. Peak G is a broad transition appearing only at $n \geq 5$; its position (684 cm^{-1}) is size-independent, but it increases in width from 90 (n = 5) to 196 cm^{-1} (n = 16). This peak correlates to the broad water librational bands at ∼700 cm^{-1} measured in liquid water thin films[34] and is also observed in the IRMPD spectra of $SO_4^{2-}(H_2O)_n$.[28] The broadness of this peak reflects the fluxionality of the numerous librational modes present in the larger hydrated bisulfate clusters. Peak H is a bending mode of the sulfate core, as observed previously in bulk studies[17] and microhydrated sulfate clusters.[28] It blue shifts monotonically with cluster size from 573 to 600 cm^{-1} (n = 1−12), beyond which it is broadened and merges with the neighboring features.

In order to elucidate the structures of these clusters, the experimental spectra are compared to simulated linear absorption spectra derived from calculated harmonic frequencies and IR intensities. These spectra, along with cluster geometries and relative energies (including zero-point corrections) are shown in Figures 2−4. The lowest-energy isomer found is shown along with one of the higher-energy isomers that shows good agreement with experiment (see Supporting Information for a complete list and tabulated frequencies). The calculated structures are generally consistent with previous results,[25,26] with some differences in energy orderings (see Table S4, Supporting

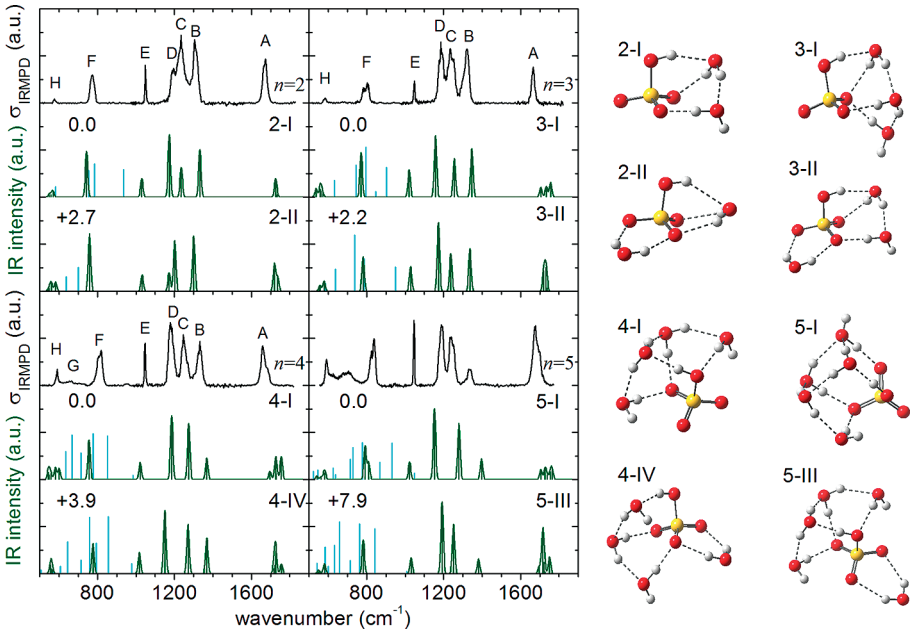

Figure 3. Comparison between experimental IRMPD spectra (top black traces) and Gaussian convolution (fwhm = 15 cm^{-1}) of the harmonic MP2/6-311+G** stick spectra (lower green traces) for n = 2−5. Water librations (blue traces) are not convoluted (see text). Structures and their relative energies (in kJ/mol) are also shown.

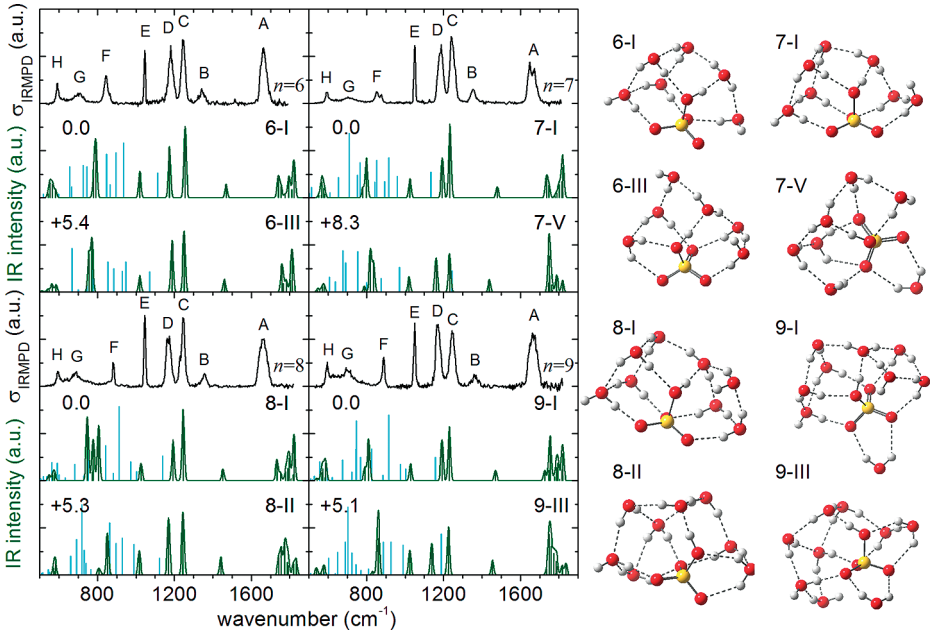

Figure 4. Comparison between experimental IRMPD spectra (top black traces) and Gaussian convolution (fwhm = 15 cm^{-1}) of the harmonic MP2/6-31+G* stick spectra (lower green traces) for n = 6−9. Water librations (blue traces) are not convoluted (see text). Structures and their relative energies (in kJ/mol) are also shown.

Information). We first consider the smallest clusters, $HSO_4^-(H_2O)_n$, n = 1−3, where specific cluster geometries can be assigned, and then examine the solvation trends in larger clusters, focusing on the spectral region corresponding to peaks B, C, and D.

The calculated spectra allow us to assign geometries to clusters with n = 1−3. The multiplet of peaks at around 1250 cm^{-1} for $HSO_4^-(H_2O)$ indicates the presence of multiple isomers. The calculated structures in Figure 2 have a bridging water molecule hydrogen bound to HSO_4^- in either a donor−donor−acceptor (DDA) or donor−donor (DD) fashion. The DDA isomer 1-I is predicted to be slightly more stable (1.6 kJ/mol) than 1-II. Structure 1-I uniquely accounts for peaks B (1309 cm^{-1}), C (1218 cm^{-1}), and D (1193 cm^{-1}), corresponding to the S═O stretching (1305 cm^{-1}), antisymmetric SO_2 stretching (1198 cm^{-1}), and SOH bending modes (1164 cm^{-1}), respectively. Variations in the frequencies of these modes in the other isomer account for

dx.doi.org/10.1021/jz200917f |J. Phys. Chem. Lett. 2011, 2, 2135–2140

the rest of the multiplet structure. A relaxed scan of the HOSO dihedral angle at the MP2/6-311+G** level yields a small 1-I → 1-II isomerization barrier (1.8 kJ/mol), suggesting that the OH group in $HSO_4^-(H_2O)$ can undergo internal rotation at room temperature. Trapping and cooling then populates both potential minima.

Figure 3 shows the BCD multiplet beginning to resolve for n = 2 and 3. In both cases, the most stable calculated structures, 2-I and 3-I, do not contain DD "bridging" water molecules (see 1-II) but instead show a hydrogen-bonded solvent network beginning from the acidic bisulfate hydrogen. However, the structures showing better agreement with experiment, 2-II and 3-II (Figure 3), are slightly higher in energy and contain a single bridging water molecule; previous DFT calculations report 2-II and 3-I as the lowest-energy structures (see Table S4, Supporting Information).[26] The width and non-Gaussian line shapes of peaks B, C, D, and F suggest the presence of both isomers in n = 2 and 3 clusters with a majority of isomer II with a minority contribution from isomer I. The calculated SOH bending frequencies for 2-II (1172 cm^{-1}) and 3-II (1331 cm^{-1}) correspond to peaks D and B, respectively, in the n = 2 and 3 experimental spectra. This abrupt blue shift in the SOH bending frequency correlates with the onset (structure 3-II) of water−water hydrogen bonding at the site of the acidic bisulfate hydrogen. This hydrogen-bonding network can facilitate partial proton transfer from the bisulfate, significantly increasing the SOH bending frequency (see below).

The remaining clusters n = 4−9 in Figures 3 and 4 show significantly fewer differences between low-lying isomers, making the assignment of cluster geometries tentative at best. For these larger clusters, we examine the trends in simulated spectra, focusing on peaks B, C, and D and their agreement with experimental results, in order to gain insight into their general solvation motifs.

We first consider peak B, the SOH bend for $n \geq 3$. The structures in Figures 3 and 4 show that bisulfate always donates a hydrogen bond to the water network, and since the motion of the SOH bend remains fairly localized even for larger clusters (see Chart S1 in the Supporting Information), peak B can probe the nature and the strength of the hydrogen bonding at this site. The intensity of peak B drops significantly for $n > 4$ as the water network begins to wrap around the bisulfate OH moiety. Two characteristic changes in the hydration network are also observed at this point. First, the water molecule accepting a H-bond from the SOH group now donates a second hydrogen bond to the water network instead of the bisulfate ion (isomers 4-I, 5-I, and 5-III). Second, we observe the onset of H-bond formation between the O-atom of the SOH moiety and a water molecule (isomers 4-I and 5-III in Figure 3). Between n = 3 and 12, the calculations show increased hydrogen bonding of the acidic bisulfate hydrogen with the solvent, as evidenced by (1) a decreasing OH stretch frequency (not shown) due to a longer OH bond and (2) an increasing bend frequency due to a narrower bending potential well. While the calculated frequencies overestimate the blue shifting of peak B, they agree qualitatively with experiment; the shifting of peak B describes the incorporation of the acidic hydrogen into the surrounding water network, the first step toward acid dissociation.

Peaks C and D, the S═O stretch and the antisymmetric SO_2 stretch, are generally well reproduced with strong intensities for most cluster sizes. Unlike the SOH bend, the normal modes for peaks C and D involve significant motion of the hydrogen-bound water network. Their frequencies also vary significantly depending on solvation structure. The symmetric SO_3 stretch at peak E, on the other hand, shows very little variation in frequency even for quite different geometries and sizes, exactly as observed in the experimental results. These factors allow us to use the frequencies of C and D and their spacing relative to E as our main selection criteria for choosing the best calculated geometries (see Table S3 in the Supporting Information for root-mean-squared errors with respect to experiment).

The other bisulfate core vibrations include the S−OH stretch (peak F) and several bending modes of the sulfate core (peak H). In the smaller clusters, peak F appears at around 750 cm^{-1}. As the cluster size increases, this vibration contains increasing contributions from the solvent network, varying in frequency and sometimes splitting into multiple peaks. The presence or absence of this splitting allows us to further eliminate some calculated structures from consideration (see Table S3 in the Supporting Information). The large blue shift and subsequent leveling out suggests that solvation increases the strength of this S−O bond until around n = 8, as evidenced by a calculated increase of the polarization of the $O^{\delta-}-H^{\delta+}$ bond with increased hydrogen bonding. The various bending vibrations that contribute to peak H are not experimentally resolved; therefore, we are content with a general agreement in peak shape for the calculated results.

The remaining peaks A and G in the spectra correspond to motions of the solvent alone and do not reveal much about the structure of the clusters. We discuss only the librational band G, which is absent from the experimental spectra up to n = 3 and then appears as a single broad structure of increasing width with increasing n, ultimately correlating to what is observed in aqueous solution. We attribute this broadening, which has previously been observed in the IRMPD spectra of other microhydrated conjugate base anions,[8] to a thermal effect. Interestingly, the calculations predict more water librational modes of appreciable IR intensity than are observed experimentally (see Figures 3 and 4 and S1−S10 in the Supporting Information), in particular for the larger clusters. This discrepancy has been observed in our previous studies of hydrated ions[8,28,35,36] and appears to be a general occurrence in the IRMPD spectroscopy of these species. The absorption of the first few photons followed by fast IVR heats the clusters up to the point where H-bonds are broken, but the clusters remain well below the dissociation limit. Consequently, the frequencies of the affected librational modes change, and the resonance condition is lost, after which no further absorption (and thus no dissociation) occurs. For this reason, normal modes involving significant librational character have been left out of the Gaussian convolutions, greatly simplifying comparison with experiment.

To summarize, comparisons between theory and experiment allow us to elucidate trends in the general solvation motif of these clusters and, in the case of clusters n = 1−3, to identify the specific isomers present. All of the clusters presented here exhibit acceptor binding of a water molecule at the acidic bisulfate hydrogen. A hydrogen-bonded water network is seen for $n \geq 3$. Beginning at $n \approx 4$, water "rings" appear as a stable solvation shell motif (see, for example, structure 6-I in Figure 4); four water molecules are linked by four hydrogen bonds to form the ring; three of these bind to the core ion. Full or partial rings add on to either side of the first ring, forming a "band" about the bisulfate, two water molecules wide. Occasionally, a structure with a single bridging water molecule is more stable (9-I in Figure 4) or agrees

better with peaks C and D in the experimental spectrum (5-III or 7-V in Figures 3 and 4). "Droplet" solvation motifs, with stacked rings and significantly fewer hydrogen bonds to the bisulfate core, are much higher in energy (see isomer 12-IV in Supporting Information).

The general solvation trends elucidated within and from studies of other systems provide an appealing and logical way to relate the acidic or basic properties of an ion in solution to its behavior in size-selected clusters. The acidic HSO_4^- favors a water molecule binding acceptor-like to the bisulfate hydrogen, as if to solvate that hydrogen and dissociate the O−H bond. Conversely, the basic HCO_3^- ion shows a strong preference for donor-like binding of the initial water molecules to the negatively charged CO_2 moiety, the first step toward deprotonation of a nearby water molecule.[36] Subsequent cluster growth happens about these first solvent molecules. The previously studied $NO_3^-(H_2O)_n$ and $HCO_3^-(H_2O)_n$ systems also show the presence of water rings beginning at $n = 4$,[35,36] while the doubly charged $SO_4^{2-}(H_2O)_n$ clusters prefer a bridging motif due to the strong ion−water interaction.[28,29]

EXPERIMENTAL AND COMPUTATIONAL METHODS

Infrared multiple photon photodissociation (IRMPD) experiments were carried out on a previously described ring electrode trap/time-of-flight mass spectrometer[37,38] using the Free Electron Laser for Infrared eXperiments (FELIX).[39] $HSO_4^-(H_2O)_n$ ions were produced by electrospray of 25 mM sulfuric acid in 1:4 water/acetonitrile solvent. A 1 M standard solution of sulfuric acid (Sigma Aldrich) was used for all dilutions. The negative ions were then transferred into a high-vacuum system. Parent ions were mass-selected in a quadrupole mass filter and focused into a ring electrode ion trap. To allow for continuous ion loading and ion thermalization, the trap was continuously filled with He gas (∼0.01−0.1 mbar) at an ion trap temperature of 15 K. After filling the trap for 99 ms, all ions were extracted from the ion trap, focused both temporally and spatially into the center of the extraction region of an orthogonally mounted linear time-of-flight mass spectrometer, and irradiated with single FELIX macropulse (50 mJ/pulse and ∼0.25% rms bandwidth). Under these conditions, most of the ions are thermalized prior to IR irradiation.[40,41] IR spectra were recorded by monitoring all ion intensities simultaneously as the laser wavelength was scanned. Bare bisulfate ions were produced but could not be dissociated. The photodissociation cross section σ was determined from the relative abundances of the parent and photofragment ions I_0 and $I(n)$ and the frequency-dependent laser power $P(\nu)$ using $\sigma = -\ln[I(\nu)/I_0]/P(\nu)$.[42]

Electronic structure calculations were performed using the Gaussian 09 program.[43] Initial cluster structures were constructed using a combination of chemical intuition and previous published results using DFT and MP2 methods with large basis sets.[25,26] The full cluster geometry was then optimized at the MP2/6-311+G** level of theory for $n = 1-5$ and at the MP2/6-31+G* level for $n = 6-12$. Frequency calculations were performed for all converged structures to test for local minima and to obtain the zero-point corrected energies reported. Structures are labeled according to their relative energies, and only those showing best agreement with experiment are shown in Figures 2−4 (many more structures are reported in the Supporting Information). The simulated infrared spectra were derived from Gaussian convolutions (fwhm = 15 cm^{-1}) of the stick spectra associated with the harmonic vibrational frequencies and linear absorption intensities. Librational modes were not included in the convolution in order to facilitate comparison with experiment. No scaling factor was used because neither a general scaling factor[44] nor a scaling factor specific to S=O double bonds[45] improved agreement with experiment for the various SO bond stretches containing both single and double bond character.

ASSOCIATED CONTENT

Supporting Information. Tabulated experimental peak positions, simulated spectra and enlarged pictures for many more bisulfate clusters with $n = 1-9$, 12. Comparison of condensed- and gas-phase IR spectra. This material is available free of charge via the Internet at http://pubs.acs.org.

AUTHOR INFORMATION

Corresponding Author

*E-mail: dneumark@berkeley.edu (D.M.N.); asmis@fhi-berlin.mpg.de (K.R.A.).

ACKNOWLEDGMENT

We thank the Stichting voor Fundamenteel Onderzoek der Materie (FOM) for granting the required beam time and highly appreciate the skill and assistance of the FELIX staff. This research is funded by the European Community's Seventh Framework Programme (FP7/2007-2013, Grant 226716). T.I.Y. and D.M.N. were supported by the Air Force Office of Scientific Research under Grant No. FA9550-09-1-0343. T.I.Y. thanks the National Science and Engineering Research Council of Canada (NSERC) for a post-graduate scholarship. Electronic structure calculations were performed at the Molecular Dynamics and Computational Facility at the University of California, Berkeley, which is supported by the NSF CHE-0840505 grant. L.J. thanks the Alexander von Humboldt Foundation for a postdoctoral scholarship.

REFERENCES

(1) Hurley, S. M.; Dermota, T. E.; Hydutsky, D. P.; Castleman, A. W. Dynamics of Hydrogen Bromide Dissolution in the Ground and Excited States. *Science* **2002**, *298*, 202–204.

(2) Oncak, M.; Slavicek, P.; Poterya, V.; Farnik, M.; Buck, U. Emergence of Charge-Transfer-to-Solvent Band in the Absorption Spectra of Hydrogen Halides on Ice Nanoparticles: Spectroscopic Evidence for Acidic Dissociation. *J. Phys. Chem. A* **2008**, *112*, 5344–5353.

(3) Sedo, G.; Doran, J. L.; Leopold, K. R. Partial Proton Transfer in the Nitric Acid Trihydrate Complex. *J. Phys. Chem. A* **2009**, *113*, 11301–11310.

(4) Flynn, S. D.; Skvortsov, D.; Morrison, A. M.; Liang, T.; Choi, M. Y.; Douberly, G. E.; Vilesov, A. F. Infrared Spectra of HCl−H_2O Clusters in Helium Nanodroplets. *J. Phys. Chem. Lett.* **2010**, *1*, 2233–2238.

(5) Re, S.; Osamura, Y.; Morokuma, K. Coexistence of Neutral and Ion-Pair Clusters of Hydrated Sulfuric Acid $H_2SO_4(H_2O)_n$ ($n = 1-5$) — A Molecular Orbital Study. *J. Phys. Chem. A* **1999**, *103*, 3535–3547.

(6) Conley, C.; Tao, F.-M. Ionic Dissociation of Hydrogen Bromide in Water Clusters: A Computational Study. *Chem. Phys. Lett.* **1999**, *301*, 29–36.

(7) Robertson, W. H.; Johnson, M. A. Molecular Aspects of Halide Ion Hydration: The Cluster Approach. *Annu. Rev. Phys. Chem.* **2003**, *54*, 173–213.

(8) Asmis, K. R.; Neumark, D. M. Vibrational Spectroscopy of Microhydrated Conjugate Base Anions. *Acc. Chem. Res.* **2011**, DOI: 10.1021/ar2000748.

(9) Eisele, F. L.; Lovejoy, E. R.; Kosciuch, E.; Moore, K. F.; Mauldin, R. L.; Smith, J. N.; McMurry, P. H.; Iida, K. Negative Atmospheric Ions and Their Potential Role in Ion-Induced Nucleation. *J. Geophys. Res., Atmos.* **2006**, *111*, D04305.

(10) Wang, X. B.; Nicholas, J. B.; Wang, L. S. Photoelectron Spectroscopy and Theoretical Calculations of SO_4^- and HSO_4^-: Confirmation of High Electron Affinities of SO_4 and HSO_4. *J. Phys. Chem. A* **2000**, *104*, 504–508.

(11) Arnold, F. Physics and Chemistry of Atmospheric Ions. In *Atmospheric Chemistry*; Goldberg, E. D., Ed.; Springer-Verlag Journal: New York, 1982; pp 273−300.

(12) Yu, F. Q.; Turco, R. P. From Molecular Clusters to Nanoparticles: Role of Ambient Ionization in Tropospheric Aerosol Formation. *J. Geophys. Res., Atmos.* **2001**, *106*, 4797–4814.

(13) Lee, S. H.; Reeves, J. M.; Wilson, J. C.; Hunton, D. E.; Viggiano, A. A.; Miller, T. M.; Ballenthin, J. O.; Lait, L. R. Particle Formation by Ion Nucleation in the Upper Troposphere and Lower Stratosphere. *Science* **2003**, *301*, 1886–1889.

(14) Sorokin, A.; Arnold, F.; Wiedner, D. Formation and Growth of Sulfuric Acid−Water Cluster Ions: Experiments, Modelling, and Implications for Ion-Induced Aerosol Formation. *Atmos. Environ.* **2006**, *40*, 2030–2045.

(15) Niedziela, R. F.; Norman, M. L.; DeForest, C. L.; Miller, R. E.; Worsnop, D. R. A Temperature- and Composition-Dependent Study of H_2SO_4 Aerosol Optical Constants Using Fourier Transform and Tunable Diode Laser Infrared Spectroscopy. *J. Phys. Chem. A* **1999**, *103*, 8030–8040.

(16) Sipila, M.; Berndt, T.; Petaja, T.; Brus, D.; Vanhanen, J.; Stratmann, F.; Patokoski, J.; Mauldin, R. L.; Hyvarinen, A. P.; Lihavainen, H.; et al. The Role of Sulfuric Acid in Atmospheric Nucleation. *Science* **2010**, *327*, 1243–1246.

(17) Querry, M. R.; Waring, R. C.; Holland, W. E.; Earls, L. M.; Herrman, M. D.; Nijm, W. P.; Hale, G. M. Optical-Constants in Infrared for K_2SO_4, $NH_4H_2PO_4$, and H_2SO_4 in Water. *J. Opt. Soc. Am.* **1974**, *64*, 39–46.

(18) Rusk, A. N.; Williams, D.; Querry, M. R. Optical Constants of Water in the Infrared. *J. Opt. Soc. Am.* **1971**, *61*, 895–903.

(19) Walrafen, G. E.; Dodd, D. M. Infra-Red Absorption Spectra of Concentrated Aqueous Solutions of Sulphuric Acid. 2. H_2SO_4 and HSO_4^- Vibrational Fundamentals and Estimates of $(F^\circ_{298.15} - H^\circ_0)/T$ and $S^\circ_{298.15}$ for H_2SO_4 Gas. *Trans. Faraday Soc.* **1961**, *57*, 1286–1296.

(20) Nakamoto, K. *Infrared and Raman Spectra of Inorganic and Coordination Compounds*, 5th ed.; John Wiley & Sons, Inc.: New York, 1997; Part A: Theory and Applications in Inorganic Chemistry.

(21) Max, J. J.; Menichelli, C.; Chapados, C. Infrared Titration of Aqueous Sulfuric Acid. *J. Phys. Chem. A* **2000**, *104*, 2845–2858.

(22) Nash, K. L.; Sully, K. J.; Horn, A. B. Infrared Spectroscopic Studies of the Low Temperature Interconversion of Sulfuric Acid Hydrates. *Phys. Chem. Chem. Phys.* **2000**, *2*, 4933–4940.

(23) Nash, K. L.; Sully, K. J.; Horn, A. B. Observations on the Interpretation and Analysis of Sulfuric Acid Hydrate Infrared Spectra. *J. Phys. Chem. A* **2001**, *105*, 9422–9426.

(24) Vchirawongkwin, V.; Kritayakornupong, C.; Rode, B. M. Structural and Dynamical Properties and Vibrational Spectra of Bisulfate Ion in Water: A Study by Ab Initio Quantum Mechanical Charge Field Molecular Dynamics. *J. Phys. Chem. B* **2010**, *114*, 11561–11569.

(25) Kurtén, T.; Noppel, M.; Vehkamaki, H.; Salonen, M.; Kulmala, M. Quantum Chemical Studies of Hydrate Formation of H_2SO_4 and HSO_4^-. *Boreal Environ. Res.* **2007**, *12*, 431–453.

(26) Nadykto, A. B.; Yu, F. Q.; Herb, J. Theoretical Analysis of the Gas-Phase Hydration of Common Atmospheric Pre-Nucleation $(HSO_4^-)(H_2O)_n$ and $(H_3O^+)(H_2SO_4)(H_2O)_n$ Cluster Ions. *Chem. Phys.* **2009**, *360*, 67–73.

(27) Zatula, A. S.; Andersson, P. U.; Ryding, M. J.; Uggerud, E. Proton Mobility and Stability of Water Clusters Containing the Bisulfate Anion, $HSO_4^-(H_2O)_n$. *Phys. Chem. Chem. Phys.* **2011**, *13*, 13287–13294.

(28) Zhou, J.; Santambrogio, G.; Brümmer, M.; Moore, D. T.; Meijer, G.; Neumark, D. M.; Asmis, K. R. Infrared Spectroscopy of Hydrated Sulfate Dianions. *J. Chem. Phys.* **2006**, *125*, 111102.

(29) Miller, Y.; Chaban, G. M.; Zhou, J.; Asmis, K. R.; Neumark, D. M.; Gerber, R. B. Vibrational Spectroscopy of $SO_4^{2-}(H_2O)_n$ Clusters, $n = 1-5$: Harmonic and Anharmonic Calculations and Experiment. *J. Chem. Phys.* **2007**, *127*, 094305.

(30) Bush, M. F.; Saykally, R. J.; Williams, E. R. Evidence for Water Rings in the Hexahydrated Sulfate Dianion from IR Spectroscopy. *J. Am. Chem. Soc.* **2007**, *129*, 2220–2221.

(31) Wang, X. B.; Sergeeva, A. P.; Yang, J.; Xing, X. P.; Boldyrev, A. I.; Wang, L. S. Photoelectron Spectroscopy of Cold Hydrated Sulfate Clusters, $SO_4^{2-}(H_2O)_n$ ($n = 4-7$): Temperature-Dependent Isomer Populations. *J. Phys. Chem. A* **2009**, *113*, 5567–5576.

(32) O'Brien, J. T.; Prell, J. S.; Bush, M. F.; Williams, E. R. Sulfate Ion Patterns Water at Long Distance. *J. Am. Chem. Soc.* **2010**, *132*, 8248–8249.

(33) Yang, X.; Wang, X. B.; Wang, L. S. Photodetachment of Hydrated Sulfate Doubly Charged Anions: $SO_4^{2-}(H_2O)_n$ ($n = 4-40$). *J. Phys. Chem. A* **2002**, *106*, 7607–7616.

(34) Zelsmann, H. R. Temperature-Dependence of the Optical-Constants for Liquid H_2O and D_2O in the Far IR Region. *J. Mol. Struct.* **1995**, *350*, 95–114.

(35) Goebbert, D. J.; Garand, E.; Wende, T.; Bergmann, R.; Meijer, G.; Asmis, K. R.; Neumark, D. M. Infrared Spectroscopy of the Microhydrated Nitrate Ions $NO_3^-(H_2O)_{1-6}$. *J. Phys. Chem. A* **2009**, *113*, 7584–7592.

(36) Garand, E.; Wende, T.; Goebbert, D. J.; Bergmann, R.; Meijer, G.; Neumark, D. M.; Asmis, K. R. Infrared Spectroscopy of Hydrated Bicarbonate Anion Clusters: $HCO_3^-(H_2O)_{1-10}$. *J. Am. Chem. Soc.* **2010**, *132*, 849–856.

(37) Goebbert, D. J.; Meijer, G.; Asmis, K. R. 10 K Ring Electrode Trap — Tandem Mass Spectrometer for Infrared Spectroscopy of Mass Selected Ions. *AIP Conf. Proc.* **2009**, *1104*, 22–29.

(38) Goebbert, D. J.; Wende, T.; Bergmann, R.; Meijer, G.; Asmis, K. R. Messenger-Tagging Electrosprayed Ions: Vibrational Spectroscopy of Suberate Dianions. *J. Phys. Chem. A* **2009**, *113*, 5874–5880.

(39) Oepts, D.; van der Meer, A. F. G.; van Amersfoort, P. W. The Free-Electron-Laser User Facility FELIX. *Infrared Phys. Technol.* **1995**, *36*, 297–308.

(40) Wende, T.; Dobler, J.; Jiang, L.; Claes, P.; Janssens, E.; Lievens, P.; Meijer, G.; Asmis, K. R.; Sauer, J. Infrared Spectroscopic Characterization of the Oxidative Dehydrogenation of Propane by $[V_4O_{10}]$. *Int. J. Mass Spectrom.* **2010**, *297*, 102–106.

(41) Jiang, L.; Wende, T.; Bergmann, R.; Meijer, G.; Asmis, K. R. Gas-Phase Vibrational Spectroscopy of Microhydrated Magnesium Nitrate Ions $[MgNO_3(H_2O)_{1-4}]^+$. *J. Am. Chem. Soc.* **2010**, *132*, 7398–7404.

(42) Oomens, J.; Tielens, A.; Sartakov, B. G.; von Helden, G.; Meijer, G. Laboratory Infrared Spectroscopy of Cationic Polycyclic Aromatic Hydrocarbon Molecules. *Astrophys. J.* **2003**, *591*, 968–985.

(43) Frisch, M. J.; Trucks, G. W.; Schlegel, H. B.; Scuseria, G. E.; Robb, M. A.; Cheeseman, J. R.; Scalmani, G.; Barone, V.; Mennucci, B.; Petersson, G. A.; et al. *Gaussian 09*, revision B.01; Gaussian, Inc.: Wallingford CT, 2010.

(44) Merrick, J. P.; Moran, D.; Radom, L. An Evaluation of Harmonic Vibrational Frequency Scale Factors. *J. Phys. Chem. A* **2007**, *111*, 11683–11700.

(45) Givan, A.; Loewenschuss, A.; Nielsen, C. J.; Rozenberg, M. Ftir and Computational Studies of Pure and Water Containing SO_3 Species in Solid Argon Matrices. *J. Mol. Struct.* **2007**, *830*, 21–34.